Chapter 3

地震断層を考慮した確率論的地震動の波形作成

3.1 地震断層を考慮した確率論的地震動の波形作成の要約

3.1.1 まえがき

　震源特性－伝播特性－地盤増幅特性を考慮して、地表面の地震動に関するスペクトル振幅を推定した。伝播特性では、従来のものを用いたが、震源特性では、断層の広がりと観測点の幾何学的関係を考慮した震源スペクトルを、地盤増幅特性では、深層地盤と浅層地盤の増幅特性を考慮した。このスペクトル振幅に適合する地震動の時刻歴波形を計算したので、概要を報告する。詳しい内容は 3.2 に記述する。

3.1.2 モデルの概要

　強震動加速度波形のフーリエスペクトル振幅 $|A(\omega)|$ に適合する加速度波形 $a(t)$ は、次式のような一様確率分布位相角を有する正弦波の級数和から計算する (Shinozuka, *et al.*1967)。

$$a(t) = W(t)\sqrt{2}\sum_{j=1}^{N_\omega}\sqrt{2\frac{1}{2\pi T_e}|A(\omega_j)|^2\Delta\omega}\cos(\omega_j t + \phi_j) \qquad (3.1-2.1a)$$

$$\omega_j = j\Delta\omega; \quad \Delta\omega = \frac{\omega_u}{N_\omega}; \quad j = 1, 2, \ldots, N_\omega \qquad (3.1-2.1b)$$

ここに、$W(t)$ は非定常特性を表現する修正関数を表わす。ここでは、大崎 (1994) の提案式を用いる。T_e は強震動の継続時間（有効継続時間：ほぼ定常部分の継続時間）で、次式から計算する。

$$T_e = \frac{L}{V_R}\left(1 - \frac{V_R}{C_S}\cos\theta\right); \qquad T_d = 2.63T_e \qquad (3.1-2.2)$$

ここに、L=地表面への断層投影長さ (km)、V_R=断層破壊速度 (km/s)、C_S=S波速度 (km/s)。T_dは強震動振幅90パーセント以上の継続時間を表わす。図3.1-1に、式（3.1-2.2）の継続時間と地震マグニチュード M の関係を久田の経験式（$\log T_d = 0.31M - 0.774$）ともに示す。式（3.1-2.2）では、$\log L = 0.5M - 1.88$、$V_R/C_S = 0.7$ を用いて図3.1-1に描いた。断層線と観測点との角度θによって継続時間に違いが生じるが、経験式は理論式のほぼ中間値を与えている。
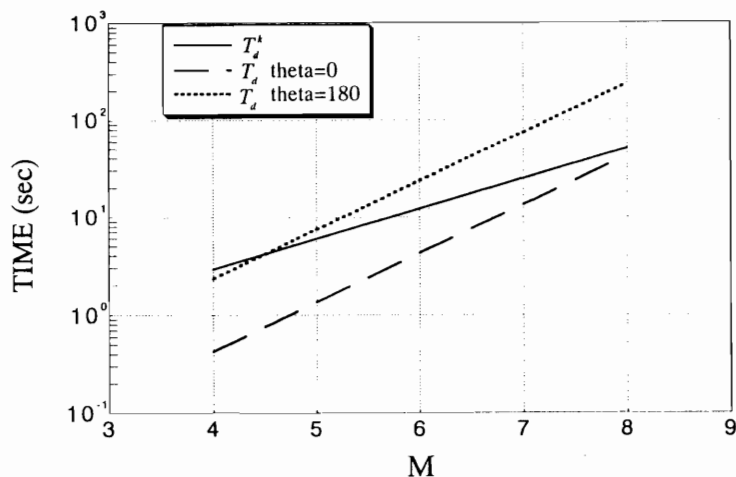

Fig.3.1-1 断層モデルによる地震動の継続時間と経験式（久田式）の比較

　強震動加速度波形のフーリエスペクトル振幅 $|A(\omega)|$ は、小地震を重ね合わせる経験的グリーン関数法の定式を基に、小地震の位相遅れ時間が大地震の破壊伝播時間 T_f の間に一様確率分布を有する確率変数として小地震を重ね合わせて求めた。

$$|A(\omega)| = SUM_N(\omega)|T(\omega)|A_0(\omega)| \qquad (3.1 - 2.3a)$$

$$|A_0(\omega)| = CA_{S0}(\omega)A_D(\omega)A_A(\omega) \qquad (3.1 - 2.3b)$$

ここに、$SUM_N(\omega)$ は小地震のランダム重ね合わせ係数を、$|T(\omega)|$ は小地震と大地震のすべり速度時間関数の比および不均質断層特性（断層面上の不均質すべりや不均質応力降下量）を考慮した伝達関数を表わし、次式で与えられる (Harada et al.,1997)。

$$T_{mn}(\omega) = \left[\frac{i\omega + \dfrac{N}{\tau}}{i\omega + \dfrac{1}{\tau}}\right]\left[\frac{1 + \kappa(\dfrac{\omega\tau}{2})^2}{1 + (\dfrac{\omega\tau}{2})^2}\right] \qquad (3.1 - 2.4a)$$

$$SUM_N(\omega) = \left[N^2\left\{1 + (N^2 - 1)|P(\omega,T_{f0})|^2\right\}\right]^{1/2} \qquad (3.1 - 2.4b)$$

$$|P(\omega, T_{f0})| = \begin{cases} 1 - c_1 \left(\dfrac{\omega}{\omega_{f0}}\right)^2 + c_2 \left(\dfrac{\omega}{\omega_{f0}}\right)^4 & 0 \leq \dfrac{\omega}{\omega_{f0}} \leq \dfrac{\pi}{2} \\ \dfrac{1}{\dfrac{\omega}{\omega_{f0}}} & \dfrac{\pi}{2} \leq \dfrac{\omega}{\omega_{f0}} \end{cases} \qquad (3.1-2.5)$$

ここに、c_1=0.16605, and c_2=0.00761. 式 (3.1-2.3) の $|A_0(\omega)|$ は小地震による観測点の地震動のスペクトル振幅を表わし、これは通常よく知られているように、ω^{-2} モデルの震源特性と伝播特性と地盤増幅特性の積として与えられる (例えば、原田ら,1995)。ここでは、地盤の増幅特性はS波速度 3-4km/s の地震基盤からS波速度 0.5-1km/s の工学基盤までの深層地盤の増幅と、工学基盤から地表面までの浅層地盤の増幅の積として、次式のように与える。

$$A_A(\omega) = \sqrt{\frac{\rho C_S}{\rho_0 C_{S0}}} \frac{\sqrt{1 + 4h_g^2 (\frac{\omega}{\omega_g})^2}}{\sqrt{(1 - (\frac{\omega}{\omega_g})^2)^2 + h_g^2 (\frac{\omega}{\omega_g})^2}} \qquad (3.1-2.6)$$

ここに、ρ, C_S は地盤の密度とS波速度を表わし、下添字は地震基盤と工学基盤の区別をするためにある。

3.1.3 加速度時刻歴の計算例と考察

ここでは、図 3.1-2 の平面図に示すような震源距離 R=30km、（震源深さ 10km）、震央距離 28.28km の 5 地点の加速度波形の例を示す。断層は長さ 20km、幅 10km の横ずれ断層とし、断層上面は地表に接するものとする。この地震の規模はマグニチュード M7.0 とし、震源は断層下面の右端とする。

図 3.1-3 は、5 地点の加速度時刻歴を示すが、断層破壊伝播方向に位置する AB 点では、加速度は大きく継続時間は短い。これらとは逆に位置する DE 点では、加速度は小さく継続時間が長い。この様な現象は地震動の指向性としてよく知られている。

この種のモデルでは、モデルパラメータ数が多いことと、それらの推定値に大きな不確定性が存在することのため、先づは、平均的パラメータ値を決めておくことが肝要である。図 3.1-4 は、AE 点のように両極端な指向性が現われる地点における断層最短距離と最大加速度の関係を海洋性地震と内陸性地震（この区別はマグニチュードと地震モーメントの関係式の違いで評価している）について描いたものと、福島・田中の経験式（実線）を示している。本モデルによる加速度は、ほぼ経験式と同じ様な距離減衰特性を示していることがわかる。今後、色々なタイプの断層モデルについて検討が必要である。
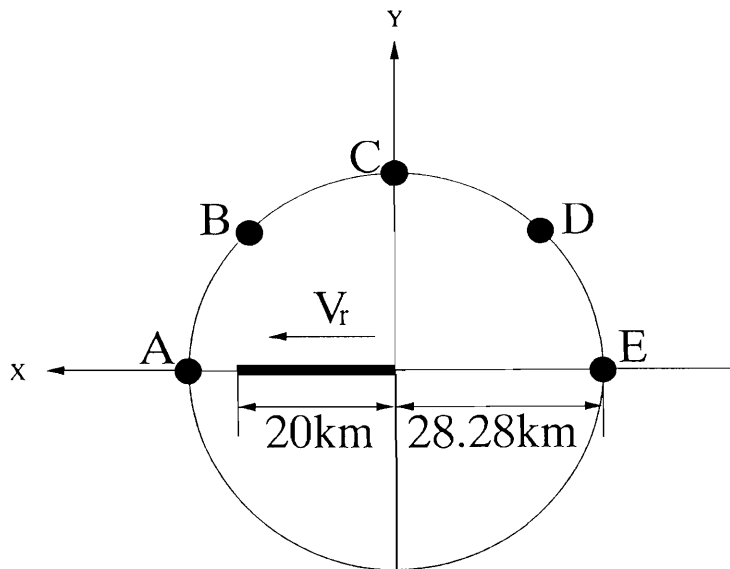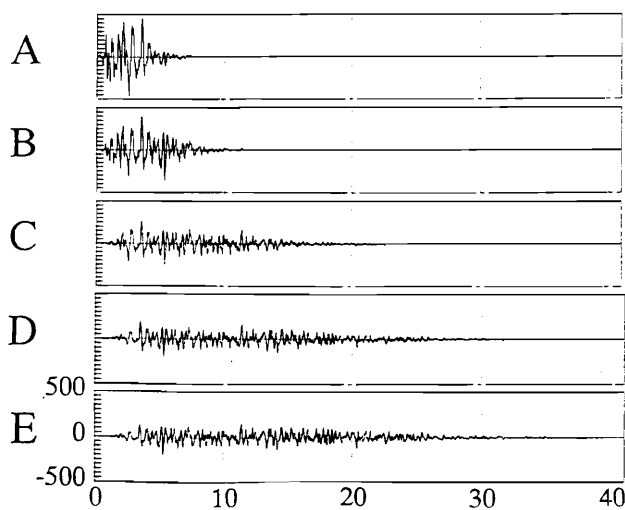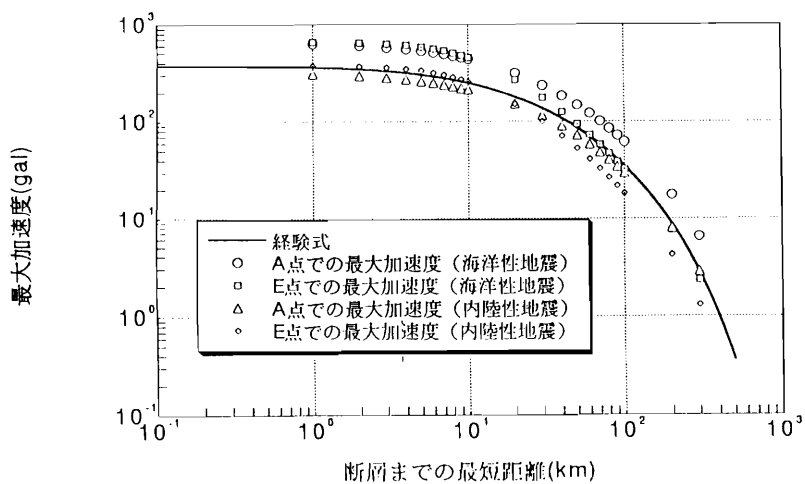
Fig.3.1-2 断層線と観測点の平面図

Fig.3.1-3 本方法による 5 地点の加速度時刻歴

Fig.3.1-4 横ずれ断層モデル（M 7 ）による加速度距離減衰特性

（計算と福島・田中経験式）

3.1.4 参考文献

1)Shinozuka, M. and Sato, Y., Simulation of nonstationary random process, Journal of the Engineering Mechanics Division, ASCE, Vol.93, No.EM1, pp.11-40, 1967.

2) 大崎順彦、新・地震動のスペクトル解析入門、鹿島出版、１９９４。

3)Harada, T. Ohsumi, T., and Darama, H., Engineering simulation of ground motions using a seismological model, Proc. of ICOSSAR'97, Kyoto, Nov. 24-28, 1997.

4) 原田隆典、田中剛、震源特性を考慮した地震動のシミュレーション手法、土木学会論文集、No.507, I-30, 209-217, 1995.

3.2 SIMULATION OF MOTIONS USING A SEISMOLOGICAL MODEL

3.2.1 INTRODUCTION

In order to simulate high frequency ground motions ($\geq$ about 1 Hz) at an average site from an average earthquake of specified size, Boore (1983) presented a stochastic method in which the Fourier spectrum amplitude (spectrum) of simulated ground motion approximates the acceleration spectrum with ω^{-2} property and a single corner frequency, which is given by physical consideration of earthquake source modeled by a point source, path, and local site effects on ground motions (Hanks and McGuire, 1981).

It is well known that a fault plane of large earthquake is too large to be treated as a point source, and the slip motion as well as stress drop are not uniform (irregular) over the fault plane for a large earthquake. These heterogeneities of the fault may cause the significant departure from the self similar ω^{-2} model of source spectrum (Aki and Richards,1980; Papageorgiou,1988).

In order to represent a kind of heterogeneity of the extended fault, the effects of source-station geometry, and the effects of propagating rupture in a simple model, Joyner and Boore (1986) considered a model where many small faults are added together with their start times distributed randomly with uniform probability over the rupture duration of the large extended fault.

In this paper, we apply the above Joyner and Boore method to the general emprical

Green's function formulation proposed by Harada, *et al.*(1995), Harada, *et al.*(1996) which is the generalization of the Irikura formulation (Irikura, 1988). Consequently, we propose an average spectrum of ground motions at a distance from a large extended fault where a kind of heterogeneity of the extended fault, the effects of source-station geometry, and the effects of propagating rupture are taken into account.

3.2.2   SPECTRUM OF GROUND MOTION FROM STOCHASTIC

Starting Equation

The starting equations in this paper belong to the empirical Green's function method initially suggested by Hartzell (1978). This method, which has been discussed in detail by Irikura (1988), is a method to simulate ground motions from an extended fault on the basis of the representation theorem of elastodynamics. Here, a brief discussion of the relevant mathematical formulation is presented in the frequency domain, and a new transfer function is presented, which accounts for the difference of the slip time functions between extended fault and small fault.

The extended fault plane with length L and width W is divided into small faults with length ΔL and width ΔW, as shown in Fig.1. Using the representation theorem of elastodynamics, the far-field displacement $u(x,t)$ in a homogeneous, isotropic, and layered medium can be expressed in the following integral form (Aki and Richards, 1980; Somerville,*et al.*, 1991):

$$u(x,t) = \sum_{m=1}^{N_L} \sum_{n=1}^{N_W} \int_{\xi_m}^{\xi_m + \Delta L} \int_{\eta_n}^{\eta_n + \Delta W} \dot{D}(\xi_m, \eta_n, t - \tau_{mn})$$

$$*G(x, \xi_m, \eta_n, t - t_{mn}) d\xi d\eta \tag{2.1}$$

where $x = (x, y, z)^T$ is the observation station, $\dot{D}(\xi, \eta, t)$ is the velocity of the source time function at position (ξ, η) on the fault, $G(x, \xi, \eta, t - t_{\xi\eta})$ is the Green's function (the impulse response of medium), and $*$ represents a convolution. τ_{mn} is the rupture propagation time from the hypocenter of the extended fault to the $(m,n)^{th}$ small fault, and t_{mn} is the propagation time for S waves to travel from the $(m,n)^{th}$ small fault to the

observation station, which are defined by:

$$\tau_{mn} = \frac{\zeta_{mn}}{V_R}; \quad t_{mn} = \frac{R_{mn} - R}{C_S} \tag{2.2}$$

where ζ_{mn} is the distance from the hypocenter of the extended fault to the $(m, n)^{th}$ small fault, R_{mn} is the distance from the $(m, n)^{th}$ fault to the observation station, R is the hypocentral distance of the extended fault, V_R is the rupture velocity of the fault, and C_S the S wave velocity of the medium. The Fourier transform of Eq.(2.1) yields the following equation:

$$\boldsymbol{u}(\boldsymbol{x}, \omega) = \sum_{m=1}^{N_L} \sum_{n=1}^{N_W} \int_{\xi_m}^{\xi_m + \Delta L} \int_{\eta_n}^{\eta_n + \Delta W} \dot{D}(\xi_m, \eta_n, \omega)$$

$$\boldsymbol{G}(\boldsymbol{x}, \xi_m, \eta_n, \omega) e^{-i\omega(\tau_{mn} + t_{mn})} d\xi d\eta \tag{2.3}$$

In order to take into account the difference of the slip time functions between the large fault and the small fault, the transfer function is introduced, which is defined as:

$$T_{mn}(\omega) = \frac{\dot{D}(\xi_m, \eta_n, \omega)}{\dot{D}_{mn}(\xi_m, \eta_n, \omega)} \tag{2.4}$$

where $\dot{D}_{mn}(\xi_m, \eta_n, \omega)$ is the Fourier transform of the velocity of the slip time function at position (ξ_m, η_n) of the small fault. Using Eq.(2.4), Eq.(2.3) can be written as:

$$\boldsymbol{u}(\boldsymbol{x}, \omega) = \sum_{m=1}^{N_L} \sum_{n=1}^{N_W} T_{mn}(\omega) \boldsymbol{u}_{mn}(\boldsymbol{x}, \omega) \tag{2.5a}$$

where

$$\boldsymbol{u}_{mn}(\boldsymbol{x}, \omega) = \int_{\xi_m}^{\xi_m + \Delta L} \int_{\eta_n}^{\eta_n + \Delta W} \dot{D}_{mn}(\xi_m, \eta_n, \omega)$$

$$\boldsymbol{G}(\boldsymbol{x}, \xi_m, \eta_n, \omega) e^{-i\omega(\tau_{mn} + t_{mn})} d\xi d\eta \tag{2.5b}$$

In Eq.(2.5b), $\boldsymbol{u}_{mn}(\boldsymbol{x}, \omega)$ is the far-field displacement due to the small fault. Equation (2.5) indicates that the motions from the large fault is the summation of the motions from the $N_L \times N_W$ small faults with the weight of $T_{mn}(\omega)$.

Based on Eq.(2.5), an approximate method can be obtained, using a single observation record $\boldsymbol{u}_0(\boldsymbol{x}, \omega)$ due to the $(m_0, n_0)^{th}$ fault. By assuming that the slip time function of each small fault and the Green's function from the position of each small fault to the observation station are approximately equal to those from the $(m_0, n_0)^{th}$ fault, then Eq.(2.5a) can be reduced as:

$$\boldsymbol{u}(\boldsymbol{x}, \omega) = \sum_{m=1}^{N_L} \sum_{n=1}^{N_W} \frac{R_0}{R_{mn}} T_{mn}(\omega) e^{-i\omega \tilde{t}_{mn}} \boldsymbol{u}_0(\boldsymbol{x}, \omega) \tag{2.6a}$$

where

$$\tilde{t}_{mn} = \tau_{mn} + t_{mn} \qquad (2.6b)$$

In deriving Eq.(2.6) the effect of the hypocentral distance on the Green's function has been considered approximately because the S wave attenuates inversely proportional to the hypocentral distance in a homogeneous isotropic medium.

From the similarity conditions of earthquakes (Kanamori *et al.*, 1975), the following relations are derived:

$$\left(\frac{M_0}{m_0}\right)^{1/3} = \frac{L}{\Delta L} = \frac{W}{\Delta W} = \frac{D}{D_0} = \frac{\tau}{\tau_0} = N \qquad (2.7)$$

where $N = N_L = N_W$, and M_0 is the seismic moment of the large fault; m_0 the seismic moment of the small fault; D and τ are the final offset of the dislocation and the dislocation rise time of the large fault, respectively; D_0 and τ_0 those of the small fault.

The transfer function $T_{mn}(\omega)$ defined by Eq.(2.4) can be obtained by specifying a slip time function. The following transfer function is used in this paper:

$$T_{mn}(\omega) = \left[\frac{i\omega + \dfrac{N}{\tau}}{i\omega + \dfrac{1}{\tau}}\right]\left[\frac{1 + \kappa\left(\dfrac{\omega\tau}{2}\right)^2}{1 + \left(\dfrac{\omega\tau}{2}\right)^2}\right] \qquad (2.8)$$

where κ is a parameter that controls the value of the transfer function in high frequency range($\omega \geq \omega_c = 2/\tau$). Although several physical models exist (Aki and Richards, 1980), the generation process of high frequency seismic waves due to fault rupture may be quite complex. Therefore, without the use of physical models, one parameter κ has been introduced here, which has to be empirically estimated. For $\kappa{=}1$, the transfer function is equivalent to that obtained by assuming the exponential function for slip time function of the large and small faults (Harada *et al.*, 1995).
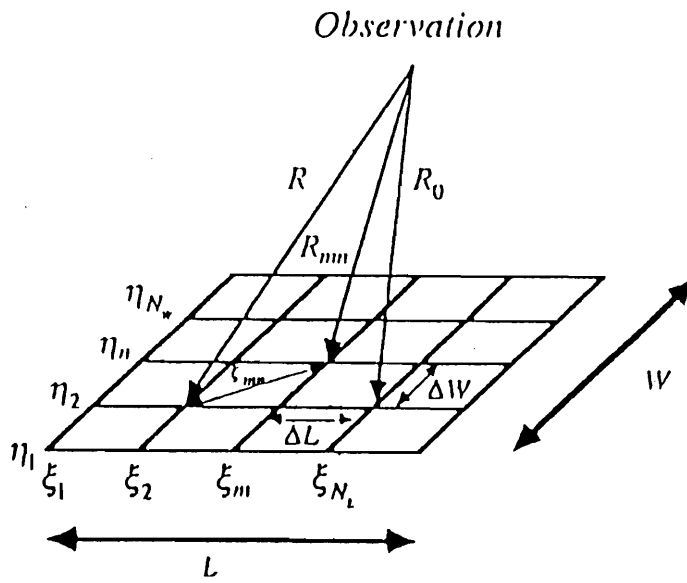
Fig.3.2-1 Schematic diagram of the Green's function method and its notation

Average characteristics of the source spectrum of an extended fault

To derive the average characteristics of the source spectrum of an extended fault, we assume that the rupture start times of each small fault are distributed randomly with uniform probability over the rupture duration T_f of an extended fault. The deterministic rupture duration is unrealistic because an average characteristics of the source spectrum are concerned in this study. Therefore the ruptute duration T_f is also assumed to be a random variable with uniform probability. By considering the practical situation, the small faults are assumed identical in average sense. For the attention of the source characteristics, we neglect the correction of the hypocentral distance. With these assumptions the Fourier spectrum of the uni- component waveform $u_S(\omega)$ from an extended fault may be written such as:

$$u_S(\omega) = \left[\sum_{m=1}^{N} \sum_{n=1}^{N} T_{mn}(\omega) e^{-i\omega t_{mn}^*} \right] u_{S0}(\omega) \tag{2.9}$$

where $u_{S0}(\omega)$ represents the Fourier spectrum of the uni-component waveform from a small fault, and t_{mn}^* the time delay uniformly distributed over the rupture duration T_f. By taking the expectation over the ensemble, the average source spectrum $|u_S(\omega)|$ is obtained as:

$$|u_S(\omega)| = SUM_N(\omega)|T(\omega)||u_{S0}(\omega)| \tag{2.10}$$

where $|T(\omega)|=|T_{mn}(\omega)|$ is the transfer function given by Eq.(2.8), and $SUM_N(\omega)$ the coefficient of random summation given by:

$$SUM_N(\omega) = \left[N^2 \left\{ 1 + (N^2 - 1)|P(\omega, T_{f0})|^2 \right\} \right]^{1/2} \tag{2.11a}$$

where

$$|P(\omega, T_{f0})| = \frac{1}{4\sqrt{3}\delta_{Tf} \left(\frac{\omega}{\omega_{f0}} \right)} \left[(\mathrm{Si}[\varpi_1] - \mathrm{Si}[\varpi_2])^2 \right.$$
$$\left. + (\mathrm{Ci}[\varpi_1] - \mathrm{Ci}[\varpi_2] - \ln[\varpi_1] + \ln[\varpi_2])^2 \right]^{1/2} \tag{2.11b}$$

where

$$\varpi_1 = 2(1 + \sqrt{3}\delta_{Tf} \frac{\omega}{\omega_{f0}}) \tag{2.11c}$$

$$\varpi_2 = 2(1 - \sqrt{3}\delta_{Tf} \frac{\omega}{\omega_{f0}}) \tag{2.11d}$$

In Eq.(2.11a) T_{f0} is the average rupture duration, and δ_{Tf} is the coefficient of variation of the random rupture duration T_f. The functions Si and Ci represent the sine integral

and the cosine integral. The first corner frequency ω_{f0} is defined in this study such as:

$$\omega_{f0} = \frac{2}{T_{f0}} \tag{2.11c}$$

The frequency variation of the function $|P(\omega, T_{f0})|$ is shown in Fig.2 for $\delta_{Tf} = 0.05, 0.3$, and 0.5. For small value of $\delta_{f0} = 0.05$, the frequency variation of $P(\omega, T_{f0})$ indicates an wavy form with peaks and troughs , similar to the behavior in the case of deterministic rupture duration $(\delta_{f0} = 0)$ where the function $P(\omega, T_{f0})$ is given by:

$$|P(\omega, T_{f0} = T_f)| = \left| \frac{\sin \dfrac{\omega}{\omega_f}}{\dfrac{\omega}{\omega_f}} \right| \tag{2.12}$$

The function of Eq.(2.12) is also shown in Fig.2. For large value of $\delta_{f0} = 0.5$, the frequency variation of $|P(\omega, T_{f0})|$ is smooth. By considering the fact that the variation in the first corner frequency ω_{f0} may be large, we propose the following simple function for $|P(\omega, T_{f0})|$

$$|P(\omega, T_{f0})| =$$

$$\begin{cases} 1 - c_1 \left(\dfrac{\omega}{\omega_{f0}} \right)^2 + c_2 \left(\dfrac{\omega}{\omega_{f0}} \right)^4 & 0 \leq \dfrac{\omega}{\omega_{f0}} \leq \dfrac{\pi}{2} \\ \dfrac{1}{\dfrac{\omega}{\omega_{f0}}} & \dfrac{\pi}{2} \leq \dfrac{\omega}{\omega_{f0}} \end{cases} \tag{2.13}$$

where $c_1 = 0.16605$, and $c_2 = 0.00761$. The function of Eq.(2.13) is also shown in Fig.2.

By introducing the second and third corner frequencies defined by,

$$\omega_c = \frac{2}{\tau}, \qquad \omega_{c0} = \frac{2}{\tau_0} \tag{2.14}$$

the transfer function of Eq.(2.8) can be rewritten as:

$$T(\omega) = T_{mn}(\omega) = \left[\frac{N + i(2\dfrac{\omega}{\omega_c})}{1 + i(2\dfrac{\omega}{\omega_c})} \right] \left[\frac{1 + \kappa(\dfrac{\omega}{\omega_c})^2}{1 + (\dfrac{\omega}{\omega_c})^2} \right] \tag{2.15a}$$

where,

$$N = \left(\frac{M_0}{m_0} \right)^{1/3} = \frac{\omega_{c0}}{\omega_c} \tag{2.15b}$$

The source spectrum of the small fault is assumed to be ω^{-2} model such as:

$$|u_0(\omega)| = \frac{m_0}{1 + (\dfrac{\omega}{N\omega_c})^2} \tag{2.16}$$

In the two extreme frequencies where $\omega \to 0$ and $\omega \to \infty$, the source spectrum of an extended fault is found from Eq.(2.10) to be given by:

$$|u_S(\omega)| = \begin{cases} N^3 m_0 = M_0 & \omega \to 0 \\ \kappa M_0 \left(\dfrac{\omega_c}{\omega}\right)^2 & \omega \to \infty \end{cases} \tag{2.17}$$

Figures 3 and 4 show the average source spectra of extended fault normalized by the seismic moment M_0 for the cases of $\kappa = 1$ and 5, respectively. In each figure, $\omega_{f0}/\omega_c = 1/10$ is assumed and the variations with the summation parameter N are shown. For comparison, the ω^{-2} source spectrum model with the second corner frequency ω_c is shown by the heavy line in each figure. It is found from Fig.3 (for the case of $\kappa = 1$) that the source spectrum of extended fault follows the ω^{-2} model at the lower frequency (ω_{f0}) and the higher frequency (ω_{c0}) ranges, but at intermediate frequency range its spectral amplitude is lower as the summation parameter N increases than that expected from the ω^{-2} model. These characteristics observed from Fig.3 are also observed from Fig.4 (for the case of $\kappa = 5$), but the source spectral amplitude is amplified by a factor of κ at higher frequency range ($\omega \geq \omega_{c0}$).

By comparing these characteristics shown in Figs. 3 and 4 with those obtained from the various irregular source models (for examples, Izutani, 1984; Papageorgiou, 1988) where the heterogeneity of either slip or stress drop on the extended fault plane is taken into account, the parameter κ may be found to be equivalent to the ratio of local stress drop to global stress drop or the ratio of dynamic stress drop to static stress drop.
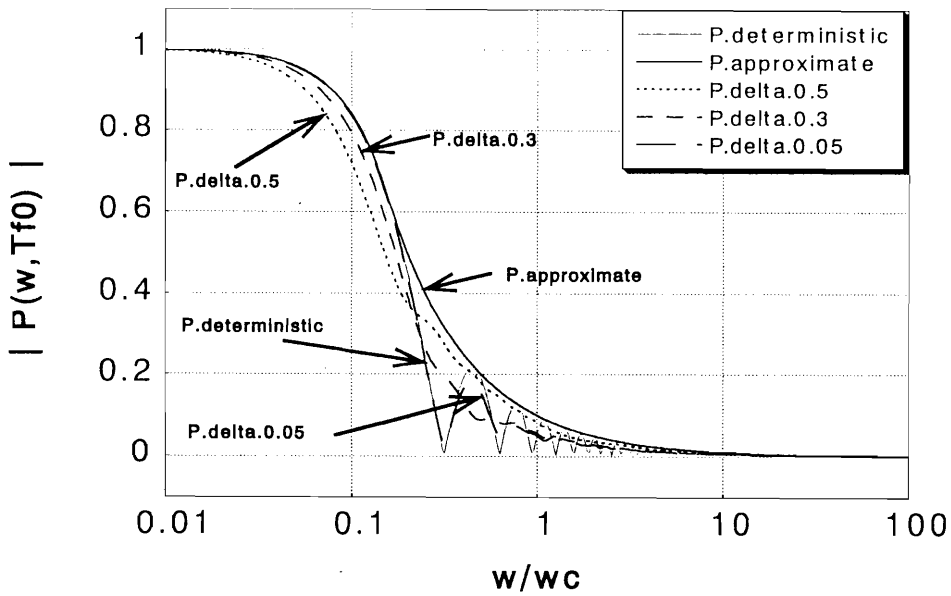
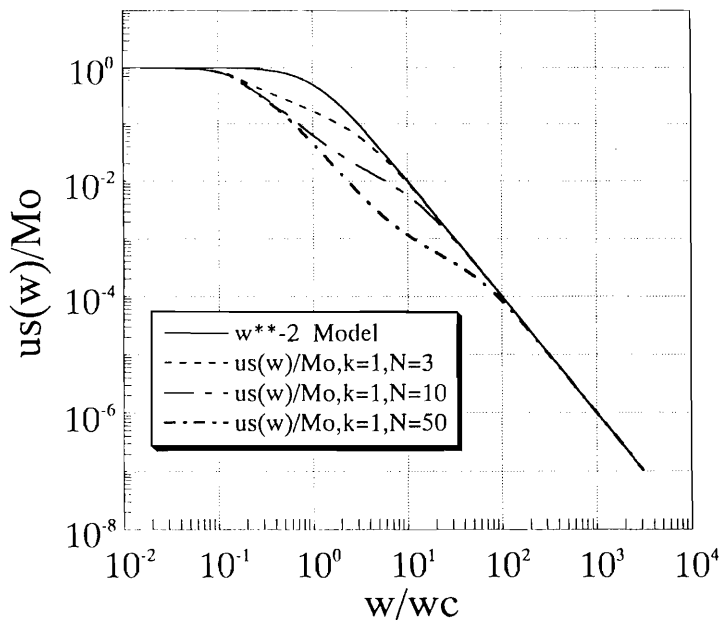Fig.3.2-2 Frequency variation of $|P(\omega, T_f)|$

Fig.3.2-3 Normalized spectra of the large earthquake by a ramdom summation of the small earthquakes, compared to the ω^{-2} spectrum (heavy line). (In the case of $\kappa = 1$)
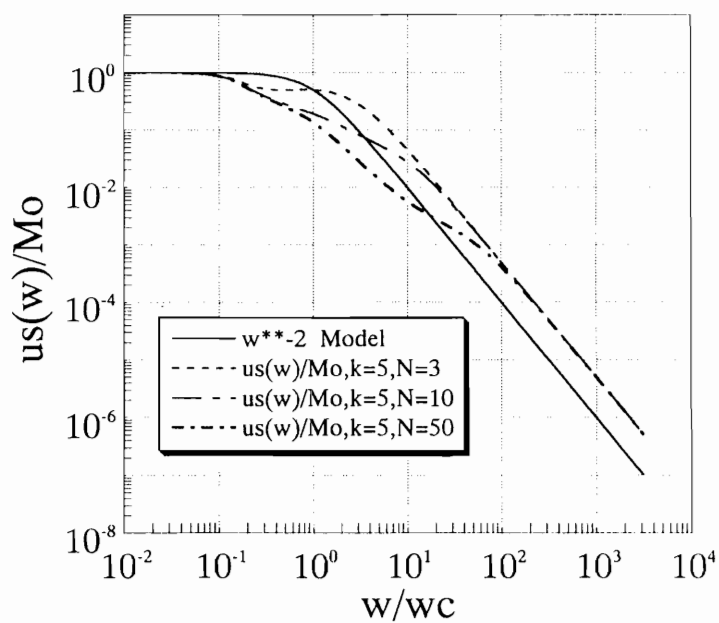
Fig.3.2-4 Normalized spectra of the large earthquake by a ramdom summation of the small earthquakes, compared to the ω^{-2} spectrum (heavy line). (In the case of $\kappa = 5$)

Average rupture duration observed at a station

The rupture duration depends on the dimensions of the fault and the rupture velocity, but it also depends on the orientation of the observation station relative to the fault. For simplicity we adopt the simplest model for the geometry of a rupture fault and the path to a observation station as shown in Fig.5. The rupture duration T_f observed at a station ($R \gg L$ where R is the hypocentral distance and L is the strike length of the fault)is given such as (Ben-Menahem, 1961):

$$T_f = \frac{L}{V_R} \left(1 - \frac{V_R}{C_S} \cos\theta \right) \tag{2.18a}$$

where θ is the azimuth angle from the strike of fault to the observation station. V_R and C_S are the rupture velocity of the fault and the S wave velocity. In Eq.(2.18a), L, V_R, C_S, and θ may be considered as random variables. However, for simplicity, we use the rupture duration of Eq.(2.18a) as an estimate of the average rupture duration:
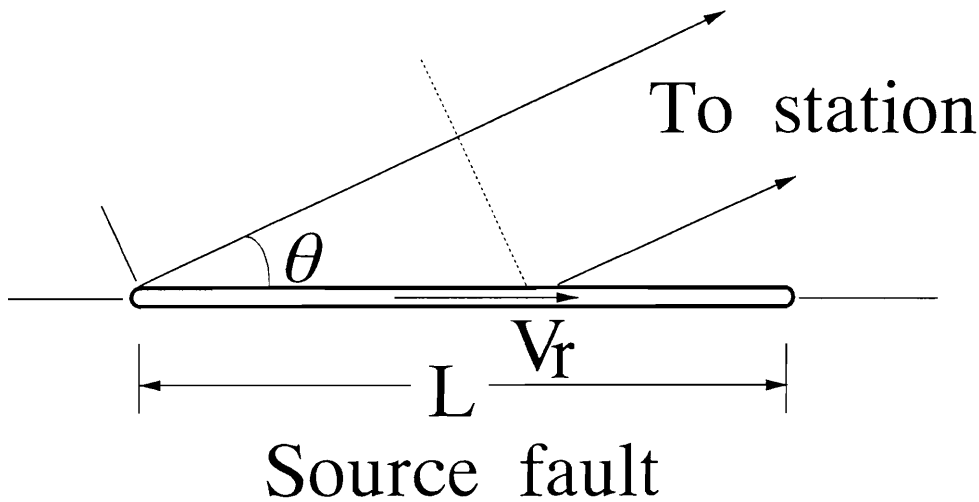
$$T_{f0} \simeq T_f \tag{2.18b}$$

Fig.3.2-5 Geometry of a rupturing fault and the path to a observation station

3.2.3   SYNTHETIC GROUND MOTION FROM STOCHASTIC

The synthetic acceleration time history of ground motion is generated using the spectral representation of stochastic waves proposed by Shinozuka (1974); Shinozuka em et

al.(1987). In this method, the power spectrum of ground acceleration have to be given, then the stationary acceleration time history is generated by the following equation:

$$a_s(t) = \sqrt{2} \sum_{j=1}^{N_\omega} \sqrt{2 S_{aa}(\omega_j) \Delta\omega} \cos(\omega_j t + \phi_j) \tag{3.1a}$$

where,

$$\omega_j = j\Delta\omega; \quad \Delta\omega = \frac{\omega_u}{N_\omega}; \quad j = 1, 2, \dots, N_\omega \tag{3.1b}$$

An upper bound of the frequency ω_u in Eq.(3.1b) represents an upper cut-off frequency beyond which $S_{aa}(\omega_j)$ may be assumed to be zero for either mathematical or physical reasons. In Eq.(3.1a), ϕ_j are independent random phase angles uniformly distributed over the range $(0, 2\pi)$. Note that the simulated time history is asymptotically Gaussian as N_ω becomes large due to the central limit theorem.

The nonstationary acceleration time history $a(t)$ is obtained by multiplying an envelope function $W(t)$ into the stationary time history $a_s(t)$.

$$a(t) = W(t) a_s(t) \tag{3.2}$$

In this study, the following expression for the envelope function is used:

$$W(t) = \begin{cases} \left(\dfrac{t}{T_b}\right)^2 & 0 \le t \le T_b \\ 1 & T_b \le t \le T_c \\ \exp[-c(t - T_c)] & T_c \le t \le T_d \end{cases} \tag{3.3}$$

where the duration (effective duration T_e)of the stationary strong portion ($T_e = T_c$ - T_b) of nonstationary ground motion is assumed equal to the average rupture duration in Eq.(2.18).

$$T_e = T_c - T_b = T_{f0} \tag{3.4a}$$

Then, the duration of nonstationary ground motion (T_d) can be given using the emprical relations by Ohsaki(1994):

$$T_d = 2.63 T_{f0} \tag{3.4b}$$

$$T_b = [0.12 - 0.04(M_{JMA} - 7)] T_d \tag{3.4c}$$

$$T_c = [0.50 - 0.04(M_{JMA} - 7)] T_d \tag{3.4d}$$

$$c = -\frac{\ln 0.1}{T_d - T_c} \tag{3.4e}$$

The power spectrum $S_{aa}(\omega)$ of ground acceleration appearing in Eq.(3.1a) is constructed using the spectrum of chapter 2. Then, $S_{aa}(\omega)$ with the effective duration $T_e = T_{f0}$ is given by:

$$S_{aa}(\omega) = \frac{1}{2\pi T_e}|A(\omega)|^2 \tag{3.5}$$

where $|A(\omega)|$ is the spectrum of ground acceleration which is given by:

$$|A(\omega)| = SUM_N(\omega)|T(\omega)||A_0(\omega)| \tag{3.6}$$

where $|A_0(\omega)|$ is the acceleration spectrum of small earthquake observed at a distance R (the hypocenter of a small earthquake is assumed to be a same place of an extended fault) with seismmic moment m_0, which is given by:

$$|A_0(\omega)| = CA_{S0}(\omega)A_D(\omega)A_A(\omega) \tag{3.7}$$

where C, $A_{S0}(\omega)$, $A_D(\omega)$, and $A_A(\omega)$, represent a scaling factor, a source spectrum, a diminution factor, and a local soil amplification factor, respectively.

The scaling factor and the source spectrum of the small earthquake are given by:

$$C = \frac{R(\theta,\varphi)FV}{4\pi\rho C_S^3}; \quad A_{S0}(\omega) = \frac{m_0\omega^2}{1+(\omega/\omega_{c0})^2} \tag{3.8}$$

where $R(\theta,\varphi)$ is the average correction factor for radiation pattern, F accounts for free-surface amplification, V accounts for the partitioning of the energy in two horizontal components, ρ is the density of the material at the source, C_S is the S wave velocity at the source, and ω_{c0} is the corner frequency of the small earthquake.

The diminution factor and the local soil amplification factor are given by:

$$A_D(\omega) = \frac{1}{1+(\omega/\omega_{max})^n}\frac{1}{R}\exp(-\frac{\omega R}{2QC_S}); \tag{3.9a}$$

$$A_A(\omega) = \sqrt{\frac{\rho C_S}{\rho_0 C_{S0}}}\frac{\sqrt{1+4h_g^2(\frac{\omega}{\omega_g})^2}}{\sqrt{(1-(\frac{\omega}{\omega_g})^2)^2+4h_g^2(\frac{\omega}{\omega_g})^2}} \tag{3.9b}$$

The first factor in $A_D(\omega)$ is the high-cut filter that accounts for the sudden drop that the spectrum exhibits above ω_{max}. It is assumed here $n = 1$. The second factor is the geometric spreading factor of the S wave. The third factor is the effect of the material damping on wave propagation in which Q is a frequency-dependent attenuation factor.

The local soil amplification factor $A_A(\omega)$ is composed of the deep soil amplification from the deep ground level near the source with the density ρ and the S wave velocity C_S to the engineering ground base with ρ_0 and S wave velocity C_{S0} of about 0.5 to 1 km/s, and the shallow soil amplification from the engineering ground base to the ground surface. The first factor in $A_A(\omega)$ of Eq.(3.9b) corresponds to the deep soil amplification factor proposed by Boore (1987), and the second factor to the shallow soil amplification represented by the Kanai-Tajimi spectrum (Kanai, 1957; and Tajimi,1960). ω_g and h_g control the peak position and the peak value of the amplification factor; $\omega_g = 15.6$(rad/sec), $h_g = 0.6$ for a firm soil.

3.2.4 NUMERICAL EXAMPLE OF SYNTHETIC GROUND MOTIONS

Numerical example is given now in order to demonstrate an applicability of the simulation method using a stochastic summation of small earthquakes to an artificial generation of strong motions for aseismic design. The example is also given to visualize the effect of directivity of seismic waves on the ground motions.

In this numerical example, the horizontal ground surface acceleration time histories on rock site are generated from an earthquake with magnitude $M_{JMA} = 7.0$ and hypocentral distance $R=30$ (km). A strike slip fault with length $L=20$ (km) and width $W=10$ (km) is considered. The hypocenter is assumed to be at the bottom edge of the fault.

The determination of the magnitude of small earthquake is arbitrary. In this study the magnitude of small earthquake M_{JMA0} is assumed to be 5.0, because the many empirical relationships in the parameters are usually obtained for the magnitude greater than about 4.0 to 5.0.

We determine the seismic moments of the earthquakes with $M_{JMA}=7.0$ and $M_{JMA0}=5.0$ by the following empirical relation which is obtained from the earthquakes occurred under the sea area around Japanese teritory (Sato, 1989):

$$M_0(\text{dyne-cm}) = 10^{(1.5M_{JMA} + 16.2)} \qquad (4.1)$$

From Eq.(2.7) the summation parameter N is determiend using the seismic moments, M_0 and m_0, of large and small erthquakes such as:

$$N = (\frac{M_0}{m_0})^{1/3} = 10 \qquad (4.2)$$

In evaluating the acceleration spectrum $|A_{A0}(\omega)|$ of ground motion from small earthquake, the following values are used:

$$R(\theta, \varphi) = 0.63; \quad F = 2.0; \quad V = 0.5; \qquad (4.4a)$$

$$\rho = 2.7\text{gr/cm}^3; \quad C_S = 3.6\text{km/sec}; \qquad (4.4b)$$

$$\omega_{c0} = 9.3\text{rad/sec}; \quad \omega_{max} = 28.7\text{rad/sec} \qquad (4.4c)$$

$$Q = 10^{(q_1 \log(\omega/2\pi) + q_2)} \qquad (4.4d)$$

where q_1=0.64, q_2=2.1.

The soil amplification of deep soil layers is assumed constant as:

$$\sqrt{\frac{\rho C_S}{\rho_0 C_{S0}}} = 2.0 \qquad (4.5a)$$

The soil amplification of shallow soil layers is evaluated using the following parameters:

$$\omega_g = 5.56\text{rad/sec}; \quad h_g = 0.6 \qquad (4.5b)$$

The ground acceleration time histories at 5 stations on rock site in Fig.6 are generated, with time interval Δt =0.01 sec, and $\omega_u = 2\pi \times 50$ rad/sec, N_ω=1024. The sample of acceleration time histories at 5 stations (M_{JMA}=7.0, R= 30km, on rock site) are shown in Fig.7. It is observed from Fig.7 that even in the same hypocentral distance R= 30 (km), the acceleration time histories are quite different from station to station in peak amplitude and duration. The higher acceleration and the shorter duration are observed in the stations A and B which are located in the direction of propagating rupture of the fault, while the lower acceleration and the longer duration in the stations D and E which are located in the oposite direction of the propagating rupture. The phenomenon observed in Fig.7 is well known as the directivity of seismic waves.
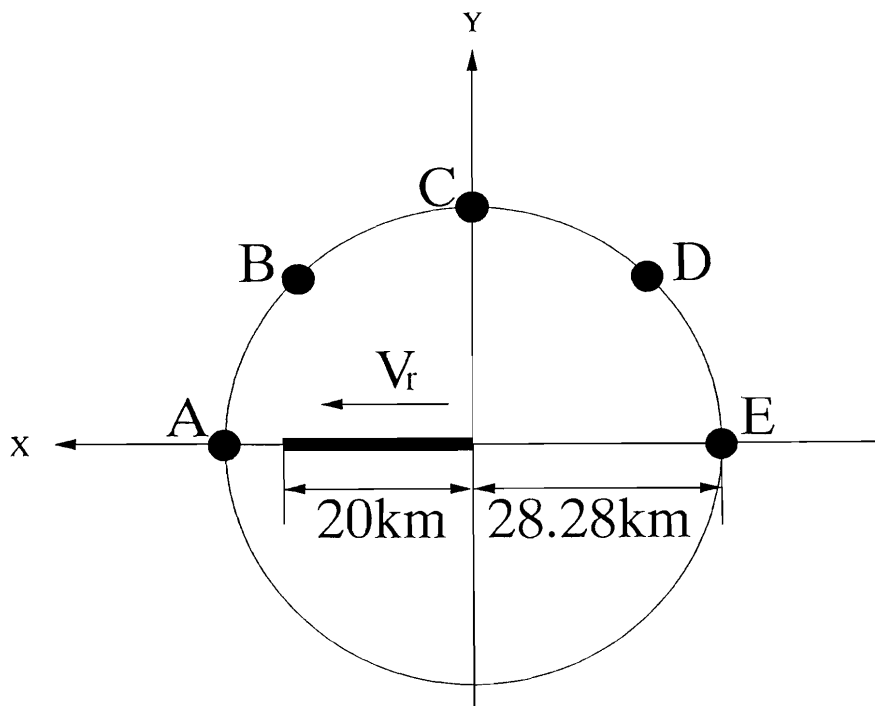
Fig.3.2-6 Plane view of the rupturing fault and the 5 stations with equal hypocentral distance
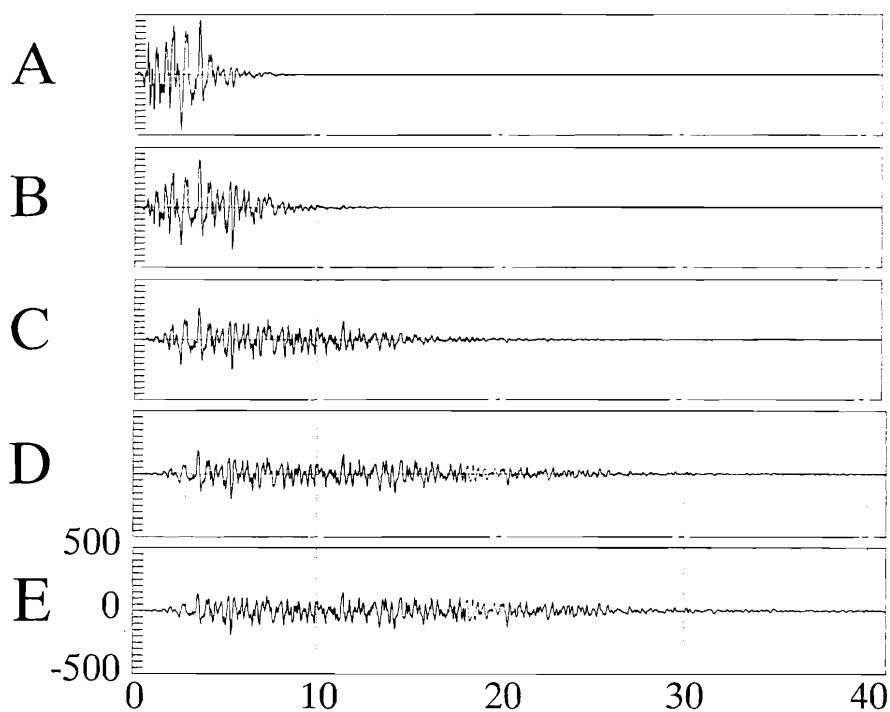

Fig.3.2-7 Sample ground acceleration time histories at 5 stations on rock site with equal hypocentral distance (M_{JMA}=7.0, R=30 km)

3.2.5 CONCLUSIONS

This paper describes a digital simulation method of strong earthquake ground motions using a seismological model. It can be concluded that:

1) Based on the representation theorem of elastodynamics for the far-field seismic waves in the frequency domain, the Fourier spectrum amplitude of ground acceleration motion from an extended fault is constructed by a stochastic summation of small earthquakes where the rupture start times of each small earthquake are distributed randomly with uniform probability over the rupture duration which is also random variable with uniform probability.

2) In the stochastic summation, a new transfer function is introduced which originally takes into account the difference of the slip time functions between the extended fault and the small fault, but also the irregular slip motion over a heterogeneous fault plane.

3) One parameter κ introduced into the new transfer function is found to be equivalent to the ratio of local stress drop to global stress drop or the ratio of dynamic stress drop to static stress drop in the available irregular source models where the heterogeneity of either slip or stress drop on the extended fault plane is taken into account.

4) The source spectrum of an extended fault by the stochastic summation have three corner frequencies, ω_{f0}, ω_c, and ω_{c0} which are related to the rupture duration of the extended fault, the rise time of the extended fault, and the rise time of the small fault.

5) Based on the spectral representation of stochastic waves, the simulation method of the nonstationary ground acceleration time histories is summarized.

6) Numerical example is given in order to make clear the procedure and the evaluation of the model parameters for the generation of ground acceleration time histories.

7) Numerical example also demonstrates the effect of the directivity of seismic waves on the acceleration time histories.

3.2.6 REFERENCES

1)Aki, K., and Richards, P.G. 1980, *Quantitative Seismology, Vol.I and Vol. II*, W.H. Freeman and Company.

2) Ben-Menahem, A. (1961), Radiation of Seismic Surface Waves from a Finite Moving

Source, *Bull. of Seism. Soc. of Am., Vol.51*, pp.401-435.

3)Boore, D.M. 1983, Stochastic Simulation of High Frequency Ground Motions Based on Seismological Models of the Radiated Spectra, *Bull. of Seism. Soc. of Am., Vol.73*, pp.1865-1894.

4) Hanks, T.C., and McGuire, R.K. (1981), The Character of High-Frequency Strong Ground Motion, *Bull. of Seism. Soc. of Am., Vol.71*, pp.2071-2095.

5) Harada, T., and Tanaka, T. (1995a), Digital Simulation of Earthquake   Ground Motions using a Seismological Model, *Journal of Structural   Mechanics and Earthquake Engineering, JSCE, No.507/I-30*, pp.209-217.

6) Harada, T., and Tanaka, T. (1996), Engineering Simulation of Ground Motions From an Extended Fault, *Proc. of the 11th World Conference on Earthquake Engineering,*

7) Harada, T., and Tanaka, T. (1995b), Digital Simulation of Ground Motions using Stochastic Green's Function and Its Verification, *Proc. of the 3rd Japan Conference on Structural Safety and Reliability*, Nobember, Tokyo, pp.527-534.

8) Hartzell, S.H. (1978), Earthquake Aftershock as Green's Functions, *Geophys. Res. Lett., Vol.5*, pp.5.

9) Irikura, K. (1988), Prediction of Strong Accelerations Motions using Empirical Green's Function, *Proc. of 7th Japan Earthquake Engineering Symposium*, pp.37-42.

10) Izutani, Y. (1984), Source Parameters Relevant to Heterogeneity of a Fault Plane, *J. Phys. Earth, Vol.32*, pp.511-529.

11) Joyner, W.B., and Boore, D.M. (1986), On Simulating Large Earthquakes by Green's Function Addition of Smaller Earthquakes, in *Earthquake Source Mechanics*, Geophysical Monograph 37, Edited by Das, S., Boatwright, J., and Scholz, C.H., American Geophysical Union, Washington, D.C., pp.269-274.

12) Kanai, K. (1957), A Semi-Empirical Formula for the Seismic Characteristics of the Ground Motions, *Bull. of Earthquake Research Institute, The University of Tokyo, Vol.35*, pp.309-325.

13) Kanamori, H., and Anderson, D.L. (1975), Theoretical Basis of Some Empirical Relations in Seismology, *Bull. of Seism. Soc. of Am., Vol.65*, pp.1073-1095.

14) Ohosaki, J. (1994), *Introduction of Spectral Analysis of Earthquake Ground Motions*, Kajima Publication, Tokyo, Japan, pp.199-201.

15) Papageorgiou, A.S. (1988), On Two Characteristic Frequencies of Acceleration Spec-

tra: Patch Corner Frequency and f_{max}, *Bull. of Seism. Soc. of Am., Vol.78*, pp.509-529.

16) Sato, R. (1989), *Handbook of Source Parameters of Earthquakes in Japan*, Kajima Publication, Tokyo, Japan, pp.82-92.

17) Shinozuka, M. (1974), Digital Simulation of Random Processes in Engineering Mechanics with the Aid of FFT Technique, In *Stochastic Problems in Mechanics*, Edited by Ariaratnam, S.T. and Leipholz, H.H.E., University of Waterloo Press, Waterloo, Canada, pp.277-286.

18) Shinozuka, M., Deodatis, G., and Harada, T. (1987), Digital Simulation of Seismic Ground Motion, *Stochastic Approaches in Earthquake Engineering*, Edited by Lin, Y.K., and Minai, R.,

Springer-Verlag, pp.252-298.

19) Somerville, P., Sen, M. and Cohee, B. (1991), Simulation of Strong Ground Motions Recorded during the 1985 Michoacan, Mexico and Valparaiso, Chile Earthquakes, *Bull. of Seism. Soc. of Am., Vol.81*, pp.1-27.

20) Tajimi, H. (1960), A Statistical Method of Determining the Maximum Response of a Building Structure during a Earthquake, *Proc. of 2nd World Conference on Earthquake Engineering,*

Vol.2, pp.781-797.